Characterization, Synthesis, and Modifications

Ultrasmall PEGylated and Targeted Core-Shell Silica Nanoparticles Carrying Methylene Blue Photosensitizer

Ferdinand F.E. Kohle, Songying Li, Melik Z. Turker, and Ulrich B. Wiesner

ACS Biomater. Sci. Eng., **Just Accepted Manuscript** • DOI: 10.1021/acsbiomaterials.9b01359 • Publication Date (Web): 20 Nov 2019

Ultrasmall PEGylated and Targeted Core-Shell Silica Nanoparticles Carrying Methylene Blue Photosensitizer

Ferdinand F. E. Kohle [†, ‡, //], Songying Li [†, //], Melik Z. Turker [†],

and Ulrich B. Wiesner [*, †]

[†]Materials Science and Engineering, Cornell University, Ithaca, NY 14853
[‡]Chemistry and Chemical Biology, Cornell University, Ithaca, NY 14853

*Department of Materials Science and Engineering, Cornell University, 330 Bard Hall, Ithaca, NY 14853.
Corresponding Author: Email: ubw1@cornell.edu, Fax: 607-255-2365.

ABSTRACT

Photodynamic therapy (PDT) presents an alternative non-invasive therapeutic modality for the treatment of cancer and other diseases. PDT relies on cytotoxic singlet oxygen (reactive oxygen species, or ROS) that is locally generated through energy transfer between a photosensitizer (PS) and molecularly dissolved triplet oxygen. While a number of nanoparticle-based PS vehicles have been described, because of their beneficial and proven biodistribution and pharmacokinetic profiles, ultrasmall nanoparticles with diameters below 10 nm are particularly promising. Here, we investigate two different particle designs deviating from ultrasmall poly(ethylene glycol) coated (PEGylated) fluorescent core-shell silica nanoparticles referred to as Cornell

prime dots (C' dots) by replacing the fluorescent dye with a photosensitizer (psC' dots), here the methylene blue derivate MB2. In the first approach (design 1), MB2 is encapsulated into the matrix of the silica core, while in the second approach (design 2), MB2 is grafted onto the silica core surface in between chains of the sterically stabilizing PEG corona. We compare both cases with regard to their singlet oxygen quantum yields, Φ_Δ, with the effective Φ_Δ^{eff} per particle reaching 111 ± 3% and 161 ± 5% for design 1 and 2, respectively, substantially exceeding single MB2 molecule performance. Encapsulation significantly improves PS photostability, while surface conjugation diminishes it, relatively to free MB2. Finally, we show that both particle designs allow functionalization with a targeting peptide, c(RGDyC). Results suggest that psC' dots are a promising targeted platform for PDT applications, *e.g.* in oncology, that may combine colloidal stability, efficient renal clearance limiting off-target accumulation, targeted delivery to sites of disease, and effective ROS generation maximizing therapeutic efficacy.

KEYWORDS: *Ultrasmall silica nanoparticles, silica chemistry, photosensitizer, photodynamic therapy (PDT), singlet oxygen quantum yield*

1. INTRODUCTION

Photodynamic therapy (PDT) has emerged as a minimally invasive and minimally toxic therapeutic modality for the treatment of cancer and other diseases.[1] The principle of PDT can generally be described in four steps: A photosensitizer (PS) is localized around diseased tissue (step 1), and activated by a light source (step 2). The absorbed photon energy leads to the generation of highly reactive singlet oxygen, $^1O_2$ (step 3), causing oxidative stress and cellular damage, eventually initiating cell death mechanisms such as necrosis and/or apoptosis in the local environment of the PS (step 4).[2] These steps impose chemical, photophysical, and structural requirements onto PDT probes.

Photophysical requirements: Generation of $^1O_2$ is caused by photoexcitation of the PS. Figure 1A depicts a simplified Jablonski scheme illustrating the photophysical processes leading to $^1O_2$ generation. From an electronically excited singlet state the PS undergoes a forbidden electron spin-flip (intersystem crossing, ISC) into an energetically lower lying excited triplet state, ^{3}PS*. From here, ^{3}PS* relaxes into the singlet ground state, ^{1}PS, via energy transfer (ET) with dissolved molecular triplet oxygen, $^3O_2$, yielding cytotoxic reactive singlet oxygen, $^1O_2$. High intersystem crossing rates (k_{ISC}) and long triplet state lifetimes ($\tau_T > 1$ μs) of the PS promote $^1O_2$ generation, which is reflected in high singlet oxygen quantum yields, Φ_Δ.[3] An ideal PS should have a molar extinction coefficient of $\varepsilon \geq 50\,000$ M^{-1} cm^{-1} in the therapeutic window of ~600–1200 nm,[3,4] and a singlet oxygen quantum yield of $\Phi_\Delta \geq 0.5$.[5] In addition, high photostability, as well as low phototoxicity in the dark are desired.[3]

Chemical requirements: Besides the general requirement of a PDT probe to be non-toxic itself, a key challenge is its localization at a specific site of interest. Singlet oxygen is highly reactive, and locally produced by the PS. Typical diffusion lengths of singlet oxygen in tissue before it reacts are on the order of only tens of nanometers.[6] Therefore, to minimize damage of healthy tissue, selective targeting is crucial. Since most PS molecules are hydrophobic and prone to aggregation in physiological environments, low selectivity towards diseased tissue and adverse pharmacokinetics have hindered their clinical translation.[4] The association of PS molecules with nanoparticles (NPs) as drug delivery systems (DDSs) can promote solubility, overcome aggregation issues to improve pharmacokinetics, and protect PSs from enzymatic degradation.[7] Furthermore, NP surface functionalization with targeting moieties reduces systemic side effects, increases the therapeutic concentration of PSs at the target site, and gives room for multi-modality platforms simultaneously enabling diagnosis, imaging, and treatment.[7] Different such NP-based DDSs have been explored, including polymeric particles, solid lipid-based materials, metal-organic framework (MOF) NPs, metallic and inorganic particles.[8-11] However, while NP-based DDSs help overcome shortages associates with the PS molecules, they themselves impose additional requirements.

Structural requirements: When PSs are loaded onto durable NPs, *i.e.* NP that are non-degrading during administration, distribution, accumulation, and elimination, it is essential that oxygen species can easily diffuse to and away from the PS molecule. Second, after NPs have targeted the site of interest and PDT has been performed (or if the NPs have failed to target the site of disease in the first place) it is necessary that NPs

are rapidly cleared from the body to reduce potential off-target toxicities (principle of *target-or-clear*).[12] Both of these requirements favor small hydrodynamic NP diameters. Given a glomerular filtration size cutoff below 10 nm hydrodynamic diameter for rapid renal clearance via the kidneys, diameters of durable NP DDSs should lie below 10 nm.[13]

In comparison to other pharmaceutical technologies, *i.e.* inhalations, transdermal patches and oral sustained release preparations, NPs are characterized by a low ratio of clinical trials to publication [14] and often fail clinical translation due to a lack of quality control, efficacy or safety.[15] A rare example for a durable NP-based DDS that is able to meet above-mentioned requirements are sub-10 nm (ultrasmall) organic-inorganic hybrid core-shell silica nanoparticles (SNPs) stabilized with polyethylene glycol (PEGylated particles). [16-18] It has been demonstrated in first published human clinical trials that such NPs efficiently target and clear from the human body, while no toxic or adverse events were observed.[19,20] This NP platform, termed Cornell prime dots or C' dots, is cost-effectively synthesized in aqueous solution and allows exceptional size and structural control on the sub-10 nanometer length scale [18,21-23] with the ability to introduce a library of targeting moieties to the surface, such as small peptide molecules or antibody fragments.[24,25] In addition, their small size in combination with a reliable steric stabilization enable sterile filtration, reducing the complexity of aseptic preparation of parenterals.

Here, we demonstrate the conversion of diagnostic fluorescent C' dots into therapeutic C' dots by covalently binding the PS molecule MB2, a derivate of methylene blue (MB) (Figure 1B and Figure S1) to ultrasmall C' dots. MB was FDA-approved [26]

and has been previously used in photodynamic therapy to treat cancerous and non-cancerous diseases.[27] MB2 has a high singlet oxygen quantum yield and maximum extinction coefficient in the near infrared ($\Phi_\Delta \approx 0.5$, $\varepsilon = 10^5$ M^{-1} cm^{-1} at about 670 nm, see Figure S1).[28] Furthermore, the optical transparency of silica and high silica matrix microporosity render SNP an ideal DDS candidate for PS molecules to be used in PDT. There have been attempts to incorporate MB into SNPs and other particle platforms.[29-31] However, in the past many attempts relied on physical incorporation of MB into large (>10 nm) SNPs and mesoporous SNPs increasing the risk of dye leakage during systemic circulation. In the following we will refer to sub-10 nm PEGylated SNP covalently binding PS molecules as photosensitizing C' dots, or simply psC' dots.

In contrast to previous studies where we encapsulated MB2 in C' dots to study the effects of spin-orbit coupling to heavier atoms like iodide co-condensed into the amorphous silica particle matrix (referred to as iodide containing C' dots, or simply iC' dots),[32] here we compare two different psC' dot designs (Figure 1C). In design 1, MB2 is encapsulated within the silica network similar to a regular dye in a typical fluorescent C' dot; in design 2, MB2 is grafted onto the SNP surface, inserted between the PEG corona chains. In both cases the PS molecules are covalently bound to the SNPs via a thiol-Michael addition click reaction between maleimide functionalized MB2 and (3-mercaptopropyl)trimethoxysilane (MPTMS) co-condensed into the silica matrix. We show that both particle types can be further functionalized with $\alpha_v\beta_3$ integrin-targeting cyclic(arginine-glycine-aspartic acid-D-tyrosine-cysteine) peptide (cRGDyC, Figure 1D and 1E) using established protocols.[33,34] Photosensitizing action is successfully demonstrated using the singlet oxygen sensor 1,3-diphenylisobenzofuran (DPBF).

Relative to free MB2, we demonstrate effective per particle singlet oxygen quantum yields of 111 ± 3% (design 1) and 161 ± 5% (design 2), respectively. These designs therefore suggest targeted and highly efficient probes for PDT which meet demonstrated physicochemical particle criteria necessary for clinical translation.[20]

2. MATERIALS AND METHODS

2.1 Materials

Aluminum-tri-sec-butoxide (ASB), (3-aminopropyl)triethoxysilane (APTES), ammonium hydroxide (28 wt% in H_2O), ammonia solution (2.0 M in ethanol), dimethyl sulfoxide (DMSO), 1,3-diphenylisobenzofuran (DPBF, 97%), hydrochloric acid (HCl, 0.5018 N in H_2O), (3-iodopropyl)trimethoxysilane (IPTMS), methylene blue (MB), (3-mercaptopropyl) trimethoxysilane (MPTMS), 2-propanol (anhydrous 99.5%), and tetramethyl orthosilicate (TMOS) were purchased from Sigma Aldrich. (3-aminopropyl)trimethoxysilane (APTMS) and methoxy-terminated poly(ethylene glycol) (PEG-silane, molar mass of ~0.5 kg/mol) were purchased from Gelest. Heterobifunctional PEG (NHS-PEG-mal, molar mass of ~960 g/mol) was purchased from Quanta BioDesign. ATTO MB2-maleimide was purchased from ATTO-Tec. Tetramethylrhodamine-5-maleimide (TMR) was purchased from AnaSpec. Ethanol (absolute anhydrous 99.5%) was purchased from Pharmco-Aaper. c(RGDyC) was purchased from Peptide International. Deionized (DI) water (18.2 MΩ·cm) was generated using a Millipore Milli-Q system. All chemicals were used as received.

2.2 Synthesis of photosensitizing C' dots according to design 1

First, 3.67×10^{-7} moles MB2 with a maleimide group were reacted with MPTMS in DMSO at a molar ratio of 1:25 (fluorophore:MPTMS) to generate a MB2-silane conjugate. To synthesize sub-10 nm PEGylated SNPs with MB2 inside the silica core, 2 mL of 0.02 M ammonia aqueous solution was first added into 8 mL of DI water yielding a pH of ~9. The solution was then stirred at room temperature for 5 min. As the silica precursor, 0.43 mmol of TMOS were added under vigorous stirring, followed by the addition of all MB2-silane. The molar ratio of MB2-silane to TMOS was about 1:1000. The solution was left stirring at room temperature overnight. Then, 0.21 mmol of PEG-silane were added and the solution was kept stirring at room temperature overnight. Finally, to promote covalent bond formation between PEG-silane and particles, stirring was stopped and the particle dispersion was heated to 80 °C for 8 hours (also see Figure 1E).[35] To remove any unreacted precursors, aggregates, or dust from the particle dispersion, particles were transferred into a dialysis membrane tube (molecular weight cutoff, MWCO = 10,000), and dialyzed in 2 L of DI water with three water exchanges every 8 hours. After dialysis, the dispersion was subject to syringe filtration (0.2 μm, Fisherbrand) and finally up-concentrated for gel permeation chromatography (GPC) using a membrane spin filter (GE Healthcare, molecular weight cutoff = 30,000) and a centrifuge at 2300 rpm.

2.3 Synthesis of photosensitizing C' dots according to design 2

Particles binding MB2 to the particle surface were synthesized according to the synthesis described for design 1, but excluding the addition of MB2-silane, or replacing

MB2 with TMR-maleimide (see main text). MB2 was added to the final silica particles by using the method of post-PEGylation surface modification by insertion (PPSMI).[24] To that end, MPTMS was added to the PEGylated particle dispersion under vigorous stirring at a concentration of 2.3 mM. The particle/MPTMS mixture was stirred at room temperature overnight, followed by the addition of 3.67×10^{-7} moles MB2-maleimide at a concentration of 37 μM. The solution was vigorously stirred at room temperature for 24 hours for the dye to react with the thiol group on the silica core surface of the particles (see Figure 1E). Afterwards, the particle dispersion was subjected to the same cleaning process as described under design 1 (dialysis, syringe filtration, GPC). Particles containing TMR on the surface were synthesized in the same way by replacing MB2-maleimide with TMR-maleimide.

2.4 Targeting peptide c(RGDyC) functionalization

Particles were peptide-functionalized with c(RGDyC)-PEG-silane (Supplementary Figure S2 in the Supporting Information). c(RGDyC)-PEG-silane was prepared by exploiting the mercapto group of cysteine of c(RGDyC) (Figure 1D) to click to the maleimide group of a heterobifunctional mal-PEG-NHS first, and then clicking the NHS to the amine group of (3-aminopropyl)trimethoxysilane (APTES). The concentration of NHS ester-PEG-maleimide in DMSO was 0.23 M. The mixed solution was left at room temperature in the glovebox for 3 hours to form silane-PEG-maleimide. After that, c(RGDyC) was added and the solution left at room temperature in the glovebox overnight to produce c(RGDyC)-PEG-silane. The molar ratio c(RGDyC):NHS-PEG-mal:APTES was 1.0:1.0:0.9. In order to functionalize particles

with c(RGDyC) peptide ligands, previously prepared c(RGDyC)-PEG-silane was added to the particle dispersion immediately before the addition of PEG-silane.[33,34] The remainder of the synthesis and purification protocol was as described before (also see Figure 1E).

2.5 Gel permeation chromatography

To remove unreacted precursors and particle aggregates from the native particle dispersion, samples were purified using gel permeation chromatography (GPC) using established protocols.[18] A BioLogic LP system with 275 nm UV detector and cross-linked copolymer of allyl dextran and N,N'-methylene bisacrylamide (Sephacryl S-300 HR, GE Healthcare) as solid phase was used. Before GPC purification each sample was up-concentrated with centrifuge spin-filters (Vivaspin with MWCO 30k, GE Healthcare) to an approximate sample volume of 600 μL, run through the column with a 0.9 wt% NaCl solution, and fraction-collected by a BioFrac fraction collector. Sample fractions were transferred to DI water by washing samples five times with centrifuge spin-filters. The resulting particles could be subjected to long-term storage in nitrogen bubbled DI water in the dark at 4 °C.

2.6 Steady-state absorption spectroscopy

Absorbance spectra were measured on a Varian Cary 5000 spectrophotometer. Spectra were measured in DI water using a quartz cuvette (HellmaAnalytics) with a 10 mm light path, and baseline corrected using a second cuvette with pure DI water as a

reference cell. All spectra were measured in 1 nm increments and peak intensities were kept between 0.01 and 0.06.

2.7 Fluorescence correlation spectroscopy

A homebuilt confocal fluorescence correlation spectroscopy (FCS) setup was used to determine particle hydrodynamic diameter, solution concentration, and number of dye molecules per particle as described previously.[36,37] Particles containing TMR dye were excited with a 543 nm HeNe laser, that was focused by a water immersion microscope objective (Zeiss Plan-Neofluar 63x NA 1.2). The fluorescence signal passed through a 50 μm pinhole and a long pass filter (ET560lp, Chroma) before being detected by an avalanche photo diode (APD) detector (SPCM-AQR-14, PerkinElmer) and auto-correlated with a digital correlator (Flex03LQ, Correlator.com). Data were fitted using a non-linear least-squares Levenberg-Marquardt algorithm and a triplet corrected correlation function, G(τ), shown in equation (1):

$$G(\tau) = 1 + \frac{1}{N_m}\left(\frac{1}{1+\tau/\tau_D}\right)\left(\frac{1}{1+\tau/(\tau_D\kappa^2)}\right)^{1/2}\frac{1}{(1-T)}\left(1 - T + T\exp\left(\tau/\tau_T\right)\right) \qquad (1)$$

Where τ is the lag time, N_m the time- and spaced-averaged number of TMR labeled particles in the FCS observation volume, that is defined by a structure factor $\kappa = \omega_z/\omega_{xy}$ with radial (ω_{xy}) and axial (ω_z) radii. τ_D is the time that a particle takes to diffuse through the observation volume. T is the fraction of TMR molecules being in the triplet state, with a triplet relaxation time, τ_T. FCS correlation curves were normalized using equation (2):

$$G(\tau) = (G(\tau) - 1)\, N_m \quad (2)$$

All samples were measured in 35 mm glass bottom dishes (P35G-1.5-10-C, Mattek Corporation) at nanomolar concentration in DI water at 20 °C, 5 kW cm^{-2} laser power, and in triplets with five 30 s long collection intervals. The observation volume was calibrated before each FCS measurement. Particle diameters, d, were calculated using the Stokes-Einstein equation (3) with the diffusion constant, D, obtained from equation (4):

$$d = 2\frac{k_B T}{6\pi\eta D} \quad (3)$$

$$D = \frac{\omega_{xy}{}^2}{4\tau_D} \quad (4)$$

The number of TMR or MB2 molecules per particle, n_m, was determined by comparing the dye concentration from steady state absorption spectroscopy, C_{Abs}, and the particle concentration measured in FCS, $\langle C \rangle_{FCS}$, using equation (5):

$$n_m = \frac{C_{Abs}}{\langle C \rangle_{FCS}} \quad (5)$$

where it was assumed that the molar extinction coefficients do not change upon dye encapsulation.

2.8 Determination of singlet oxygen quantum yields

Singlet oxygen quantum yield, Φ_Δ, measurements were carried out in ethanol with 1,3-diphenylisobenzofuran (DPBF) as a detector molecule for trapping singlet oxygen. The generation of singlet oxygen could be observed by a reduction of the DPBF

absorption band at 410 nm. Measurements were carried out at sample optical densities of 0.15 – 0.50 in a 100 µL quartz cuvette (Starna). Samples were evenly exposed to a 635 nm, expanded, and collimated laser beam of a solid-state laser (Power Technology Inc.) at 3 mW/cm^2 with a spot size of about 1 cm in the same cell. To acquire a 0.5 - 0.6 absorption, DPBF was added at a concentration of approximately 18.75 µM. All absorption spectra were measured in 1 nm steps and baseline-corrected against a second cuvette with ethanol as a reference cell. The sample absorption was recorded at defined time intervals and corrected for the sample absorption spectrum in the absence of DPBF. Φ_Δ was calculated by comparing all samples to the standard methylene blue (MB) dye with known singlet oxygen quantum yield of Φ_Δ = 0.52 (in ethanol)[38] by plotting the natural logarithm of the reduction of the 410 nm DBPF band against the exposure time and using equation (6), where m represents the slope of a linear fit through the data points:

$$\Phi_\Delta(sample) = \Phi_\Delta(MB)\frac{m(sample)}{m(MB)} \quad (6)$$

To determine the effective singlet oxygen quantum yield, Φ_Δ^{eff}, the particle concentration as determined by FCS and the MB concentration were matched. Errors were calculated by determining Φ_Δ three separate times for one sample.

2.9 Transmission Electron Microscopy (TEM)

1 µL of a ~15 µM concentrated sample solution (design 1, PEG-MB2-psC' dots, and design 2, MB2-PEG-psC' dots) was diluted into 100 µL DI water. ~10 µL of the

diluted solution was then dropped onto carbon-film-coated TEM copper grids (Electron Microscopy Sciences), and allowed to air dry. TEM imaging was performed using a FEI Tecnai T12 Spirit microscope operated at 120 kV.

2.10 Photostability Measurements

Measurements were carried out in DI water using a 100 μL quartz cuvette (Starna). All samples (design 1, PEG-MB2-psC' dots, and design 2, MB2-PEG-psC' dots) were measured at optical densities of ~0.01 to ~0.02 with respect to the monomer peak, and were evenly exposed to a Diode Red 640 nm Laser (Opto Engine LLC) expanded and collimated solid-state laser (Inc.) at 50 mW/cm^2 with a spot diameter of about 1 cm in the same cell. All absorption spectra were measured in 1 nm steps and baseline-corrected against a reference cell containing DI water. The absorption of each sample was recorded at exposure times of 10 s, 20 s, 30 s, 30 s, 60 s, 120 s, 240 s, 480 s, 900 s, 1800 s and 3600 s. Spectra were qualitatively interpreted by fitting the absorption spectrum with two Gaussians representing the monomer and dimer peaks.

3. RESULTS AND DISCUSSION

3.1 Synthesis of Photosensitizing C' dots

Photosensitizing C' dots (psC' dots) covalently encapsulating the methylene blue derivate MB2 inside the particle (design 1, Figure 1C and 1E) were synthesized by combining tetramethylorthosilicate (TMOS) and MB2-silane (Figure 1B) in basic

aqueous solution. After particle formation, further particle growth was quenched by the addition of PEG-silane (Figure 1B) to the reaction mixture, which was subsequently heated to promote covalent bond formation between PEG-silane and surface silanol groups.[18,35] Particles containing MB2 on the particle surface (design 2, Figure 1C) were synthesized in the same way, however, MB2 was attached using a grafting method referred to as post-PEGylation surface modification by insertion (PPSMI).[24] This method employs sulfhydryl-reactive click chemistry, by adding thiol-silanes below the nucleation threshold into an aqueous dispersion of PEGylated SNPs. The small molar mass silane precursors diffuse through the PEG corona chains and react with the silica core particle surface. The pending amine or thiol groups can further be reacted with maleimide functional groups.[24] For design 2, we used (3-mercaptopropyl) trimethoxysilane (MPTMS) to functionalize the particle surface with thiol groups to click MB2-maleimide to the particle (Figure 1E). Finally, all particles were cleaned from unreacted precursors and particle aggregates via gel permeation chromatography (GPC) prior to further characterization (see Materials and Methods section).

3.2 Particle Characterization

Fluorescent correlation spectroscopy (FCS) is a powerful tool for the development and characterization of ultrasmall fluorescent silica nanoparticles.[36,37] FCS probes particle behavior with high signal-to-noise, and enables to assess a number of sample properties simultaneously including particle concentration, hydrodynamic size, and particle brightness. Particle diameter and concentration are determined by measuring the fluorescence fluctuations of particles diffusing through a well-defined observation volume of a laser beam and subsequently auto-correlating the fluorescence

time signals. In combination with steady-state absorption measurements of the same sample, the number of fluorescent molecules can then be determined.

However, due to the weakly-emissive nature of MB2 (Supplementary Figure S3 in the Supporting Information), fluorescence-based size determination of MB2 functionalized particles by FCS was not possible. To render MB2-containing particles accessible to FCS characterization, particles were co-functionalized with the fluorescent dye conjugate tatramethylrhodamine-silane (TMR-silane) (Figure 1B). For design 1 with encapsulated MB2 we grafted TMR onto the particle surface using PPSMI. For design 2 we turned the situation around: We synthesized SNPs encapsulating TMR dye before MB2 was grafted on the particle surface (Figure 1E). A combination of FCS and steady state absorption spectroscopy was then used to determine the number of MB2 and TMR molecules per particle. The resulting FCS correlation curves were fitted with a correlation function (see equation (1), Materials and Methods) from which the time averaged number of particles and the diffusion constant were extracted. To determine the number of dyes per particle, the dye concentration as determined by steady-state absorption spectroscopy was compared to the concentration of the particles as determined by FCS (equation (5), Materials and Methods), yielding the average number of dyes per particle. For accurately determination of the number of MB2 dyes per particle, it is necessary that every MB2 containing particle carries at least one TMR dye, a requirement that is not necessarily met. We accounted for that to the best possible degree by working with high TMR concentrations in the synthesis. Dye molecules that were not covalently bound during synthesis were washed away by dialysis and separated from the particles by GPC. Supplementary Figure S4A and S4B in the Supporting

Information show the GPC elugrams before and after TMR and MB2 surface functionalization of particles, respectively. Both elugram-pairs show a single peak and were congruent to each other, indicating that TMR dye molecules (design 1), or MB2 dye molecules (design 2) were grafted onto the respective SNP surface.

Figure 2A and 2B show the FCS correlation curves of the fluorescent particles containing the photosensitizer MB2. The curves were fitted using a triplet corrected translational diffusion correlation function (equation (1), Materials and Methods). Particle hydrodynamic diameters of 5.9 nm for MB2 encapsulating C' dots with TMR surface functionalization (TMR-PEG-MB2-psC' dots), 5.2 nm for TMR encapsulating C' dots (PEG-TMR-C' dots), and 5.2 nm for TMR encapsulating C' dots with MB2 surface functionalization (MB2-PEG-TMR-psC' dots) were obtained (a comprehensive nomenclature to describe C' dots is presented in the supporting information of reference *24*). For comparison, TEM images of particles of design 1 and 2 were taken. As expected, due to the low contrast of the PEG corona and hydration layer slightly smaller particle diameters of about 4.0 nm were determined for both designs, (Supplementary Figure S5A and S5B).

Figure 2C and 2D show the UV-vis absorption spectra of PEG-MB2-psC' dots, TMR-PEG-MB2-psC' dots, PEG-TMR-C' dots, and MB2-PEG-TMR-C' dots in water, respectively. For comparison, the absorption spectra of TMR-maleimide and MB2-maleimide are superimposed onto the particle spectra. For TMR-PEG-MB2-psC' dots and MB2-PEG-TMR-psC' dots, a TMR absorption peak can be observed indicating successful functionalization of particles with TMR and MB2, respectively.

Comparing the absorption profiles of MB2 for the two different designs, a relative hypsochromic shift (blue-shift) from 668 nm to 644 nm of the main peak for design 1 relative to free MB2 is observed that is absent in design 2. This hypsochromic shift likely originates from dimethylation of the auxochrome groups of MB2, from -$N(CH_3)_2$ to -$NH(CH_3)$ and/or -NH_2, which is promoted in basic media.[39,40] In addition, both designs display a heightened left shoulder in the absorption peak as compared to free MB2 dye that is more pronounced in design 1 than it is in design 2. The heightened shoulders around 620 nm and 605 nm for design 2 and one, respectively, are a result of dimerization of MB2 at high concentrations (1×10^{-6} to 4×10^{-4} M) in aqueous media (MB2 concentration during synthesis is $3.67x10^{-5}$ M).[41] MB monomers and dimers are known to have distinct absorption peaks located at 664 nm and 590 nm, respectively, with an equilibrium constant of $3.8x10^{3}$ M^{-1} in water.[42] However, the formation of dimers is not only dependent on concentration but is additionally promoted by the presence of oppositely charged surfaces.[43] For design 1, the cationic MB2 sensitizer was added to the synthesis during the silica particles formation and hence was exposed to negatively charged silica nucleation seeds/clusters (at pH 9). For design 2, MB2 was grafted onto the PEGylated silica particle surface at neutral conditions (pH 7), consequently showing no peak shift and relatively fewer MB2 dimers, despite the same MB2 concentration during the synthesis as for design 1.

To determine the number of MB2 molecules per particle we compared the particle concentrations estimated by FCS and the MB2 concentrations from steady-state absorption measurements. For practical reasons, we assumed that the extinction coefficient remained unaffected in the particle synthesis. This is not necessarily true due

to the metachromatic nature of methylene blue and demethylation. Nevertheless, based on this assumption we estimated the average number of dyes per particle (equation (5), Materials and Methods) to be 2.4/3.3 for MB2/TMR for design 1 and 3.4/2.3 for MB2/TMR for design 2.

3.3 Determination of Singlet Oxygen Quantum Yields

Next, we measured the singlet oxygen quantum yield, Φ_Δ, for both particle designs using the singlet oxygen sensor 1,3-diphenylisobenzofuran (DPBF). For these measurements, we matched the particle concentrations as determined by FCS to yield an effective singlet oxygen quantum yield per psC' dot (Φ_Δ^{eff} (psC' dot)). Figure 3A demonstrates the principle of oxygen sensing using DPBF and the particle TMR-PEG-MB2-psC' dots (design 1) in ethanol. The mixture is evenly exposed to an expanded and collimated 635 nm laser beam for defined time intervals. The singlet oxygen that is generated by the psC' dots reacts with DPBF molecules, yielding 1,2-dibenzoylbenzene (Figure 3A inset).[44] The formation of 1,2-dibenzoylbenzene was monitored via a reduction of the absorption band at 410 nm (Figure 3B). By comparing samples to a methylene blue standard (Φ_Δ(MB) = 0.52), Φ_Δ^{eff}(psC' dot) was determined (see equation (6), Materials and Methods), resulting in values of 111 ± 3% for design 1 (TMR-PEG-MB2-psC' dots) and 161 ± 5% for design 2 (MB2-PEG-TMR-psC' dots). This translates to an estimated per dye singlet oxygen quantum yield of 46% and 47%, respectively, based on the estimated number of MB2 dyes per particle. The slightly lower values for Φ_Δ of the dyes associated with the particles versus free methylene blue dye can be rationalized by the steric shielding effects of encapsulation or grafting within the PEGylation corona. The silica network and/or the PEG molecules shield diffusing

oxygen, first, from MB2, and then, from DPBF resulting in a reduced singlet oxygen quantum yield. Although for both designs the per dye Φ_Δ values are similar, surface grafted MB2 molecules are likely less shielded than dyes fully encapsulated in the silica network. In addition, it is known that methylene blue dimers and monomers engage in different photochemical processes. While monomers undergo energy transfer reaction with triplet oxygen, dimers engage in electron transfer reactions with other methylene blue molecules.[43] These different energy dissipation pathways of dimers correlate negatively with the singlet oxygen quantum yield possibly also contributing to the slightly reduced singlet oxygen quantum yield per dye molecule of design 1 and design 2.[45] However, relative to a single MB2 molecule, the multiplicity effect stemming from multiple MB2 molecules colocalized on one particle far overcompensates for a reduced per dye singlet oxygen quantum yield by steric shielding and/or dimerization.

To exclude the possibility of $^1O_2$ formation in the absence of irradiation with light (dark toxicity) for the different particle designs, we repeated singlet oxygen quantum yield measurements, but did not expose the samples to the laser beam. Supplementary Figure S6 in the Supporting Information shows results of the same experiment as shown in Figure 3A for design 1 (PEG-MB2-psC' dots). This time, the DPBF peak at 410 nm remains unchanged, however, indicating no formation of 1,2-dibenzoylbenzene and hence no generation of singlet oxygen. This is the case for both designs.

To qualitatively investigate how MB2-particle encapsulation influences MB2 photostability we performed photobleaching experiments comparing free MB2 to particles of design 1 and design 2 in aqueous solution. Samples were exposed to an

expanded and collimated 640 nm laser for defined time intervals and bleaching progression was recorded via steady state absorption spectroscopy (Figure S7A to S7C). To distinguish the MB2 monomer bleaching from the dimer peaks we fitted the spectra with two Gaussians (Figure S7D to S7F). We found that MB2 monomer dye incorporated in the silica matrix bleaches substantially slower compared to free MB2 dye in solution (Figure S7G and S7H). This agrees with previous findings where it was shown that incorporated organic dyes are shielded from dissolved oxygen.[46] On the other hand, MB2 dyes grafted onto the particle surface had a tendency to bleach faster as compared to free MB2 dye. This could possibly be understood by the presence of a higher per particle dye average of MB2 molecules on the particle surface, leading to an effectively increased local concentration of MB2 dyes around the particle.

3.4 Functionalization of psC' dots with c(RGDyC)

Specific targeting of photosensitizers to diseased tissue increases the efficacy of PDT and minimizes collateral damage to healthy tissue. Here, we functionalized psC' dots with the targeting moiety cyclo(arginine-glycine-aspartic acid-D-tyrosine-cysteine) (c(RGDyC)) (Figure 1C), which targets $\alpha_v\beta_3$ integrins overexpressed, e.g. on various cancer cells including melanoma.[20] It has been shown that the endocytosis-mediated cellular uptake of c(RGDyC)-functionalized particles correlates with the $\alpha_v\beta_3$-expression levels of cells,[47,48] and increases the intracellular particle concentration, rendering c(RGDyC) a specific targeting moiety with high affinity for the treatment of melanoma.[12,34] In previous studies, it could be shown that ultrasmall c(RGDyC)-functionalized SNP (Cornell dots) demonstrated selective disease targeting in

combination with bulk renal clearance in human clinical trials.[20] We therefore believe that c(RGDyC)-functionalized psC' dots are a relevant first model system.

Particles were functionalized by adding c(RGDyC)-PEG-silane (Figure 1E and Supplementary Figure S2 in the Supporting Information) during the PEGylation step (for details see Materials and Methods).[18] To allow more steric freedom for ligand binding to integrins, the c(RGDyC)-PEG-silane was chosen to be three ethylene oxide (EO) units longer than the PEG-silane (twelve versus six to nine units). Due to the weakly-fluorescent nature of MB2, a FCS analysis could not be conducted. Instead we compared the GPC elugrams before and after peptide functionalization for particle design 1 (PEG-MB2-psC' dots and c(RGDyC)-PEG-MB2-psC' dots), and design 2 (MB2-PEG-psC' dots and MB2-c(RGDyC)-PEG-psC' dots) (Supplementary Figures S8A and S8B in the Supporting Information). In both cases, we observed single peaks that were congruent to each other. All particles were then characterized using steady-state absorption spectroscopy. Figures 4A and 4D show the absorption spectra of design 1 and design 2, respectively, with and without c(RGDyC)-functionalization in water. In both cases, increased absorption between 200 and 300 nm was noticeable. Due to strong absorption features in that region it is difficult to clearly identify the peptide absorption by qualitative comparison. For that reason, we subtracted the two spectra from each other and displayed the difference spectra in Figures 4B and 4E. In both cases a band at ~260 to 270 nm can clearly be identified, which coincides with the absorption band of the c(RGDyC) spectrum (Supplementary Figure S8C in the Supporting Information).[24] Using the relative absorption peaks of tyrosine in c(RGDyC) and of MB2, we estimated

17 and 14 c(RGDyC) units per MB2 molecule for design 1 and design 2, respectively, which is close to the desired number based on earlier studies.[34]

Finally, we tested the effect of c(RGDyC)-functionalization on the relative singlet oxygen quantum yield performance. We compared particles with and without c(RGDyC) for absorption matched samples of the same design. For both designs we measured a reduction of singlet oxygen quantum yield by a relative 25% for design 1 and by a relative 12% for design 2 (Figure 4C and 4F). This finding is surprising. Given the spatial proximity of surface MB2 and c(RGDyC), one would expect a stronger effect of c(RGDyC) in design 2. Results suggest, however, that c(RGDyC) increases the steric shielding more significantly for the encapsulated MB2 than for the surface grafted MB2.

4. CONCLUSIONS

In this study, we have presented two different designs for the covalent loading of ultrasmall organic-inorganic hybrid silica nanoparticles with photosensitizer molecules (psC' dots) in the form of methylene blue derivate MB2. MB2 was either covalently encapsulated in the silica core or attached to the silica core surface. Both designs yielded sub-10 nm size particles that could be further functionalized with c(RGDyC) as a targeting moiety. We found that the properties of MB2 strongly depend on its position in the particle. While design 1 protected MB2 from photobleaching, design 2 showed increased photobleaching as compared to free MB2 dye. Despite slightly reduced per molecule singlet oxygen quantum yields of MB2 upon particle association, the effective per particle singlet oxygen quantum yields far exceeded the

quantum yield of a single MB2 dye as a result of multiple MB2 molecules per particle. The advantages established for fluorescent dye encapsulating C' dots and expected for ultrasmall organic-inorganic hybrid psC' dots as a delivery and protective system for photosensitizers make such probes interesting candidates for applications in PDT: This includes surface PEGylation providing particle stability, *e.g.* in blood serum, surface targeting moieties enabling enhanced accumulation at desired sites of disease, and ultrasmall particle size enabling rapid renal clearance thereby minimizing possible side effects.[20]

Although this study focuses on the photosensitizer MB2, described design principles and synthesis methods are in principle applicable to other photosensitizers. This might be of special interest for hydrophobic NIR and IR photosensitizers with large singlet oxygen quantum yields, *i.e.* porphyrins, chlorins, phthalocyanines, naphthalocyanines, bacteriochlorins, and BODIPY dyes. PEGylated silica can provide a water-soluble carrier for these cargos, to allow specific targeting and achieve high local concentrations at targeted sites, while avoiding aggregation in aqueous media. While more work is necessary to fine-tune such synthesis protocols to fully harvest the potential of ultrasmall organic-inorganic hybrid silica nanophotosensitizers (psC' dots), we believe that psC' dots carry high potential for clinical translation.

FIGURES

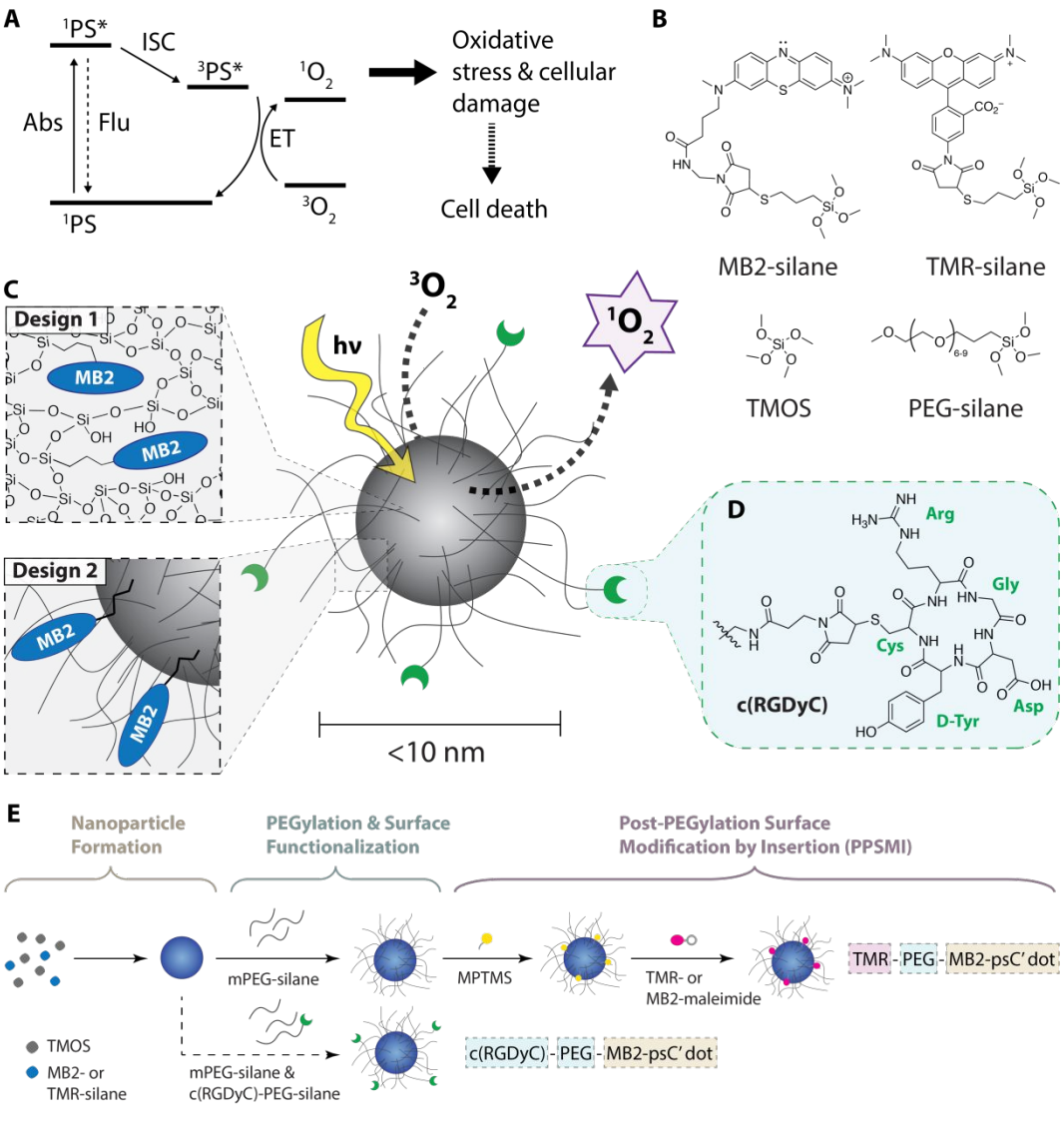

Figure 1. (A) Simplified Jablonski diagram illustrating the creation of reactive singlet oxygen, $^1O_2$. ^{1}PS denotes the singlet ground state, ^{1}PS* the electronically excited singlet state, and ^{3}PS* the electronically excited triplet state of a photosensitizer. $^3O_2$ denotes the triplet ground state of molecularly dissolved oxygen. (B) Precursor molecules for the synthesis of sub-10 nm silica nanoparticles, showing the methylene blue derivate MB2-silane, the rhodamine dye TMR-silane, tetramethyl orthosilicate (TMOS), and polyethylene glycol-silane (PEG-silane). (C) Schematic representation of two different designs of functionalized photosensitizing sub-10 nm silica nanoparticles (psC' dots). Design 1: Covalent encapsulation of one or more MB2 molecules in the silica matrix of the particle core (PEG-MB2-psC' dots). Design 2: Particle surface functionalization with one or more MB2 molecules (MB2-PEG-psC'dot). (D) Molecular structure of targeting moiety cyclo(Arg-Gly-Asp-D-Tyr-Cys) (cRGDyC). (E) Synthesis scheme for

functionalized sub-10 nm silica photosensitizers of design 1 and 2 showing the three general synthesis steps. A comprehensive nomenclature to describe C' dots is presented in the supporting information of reference *24*.

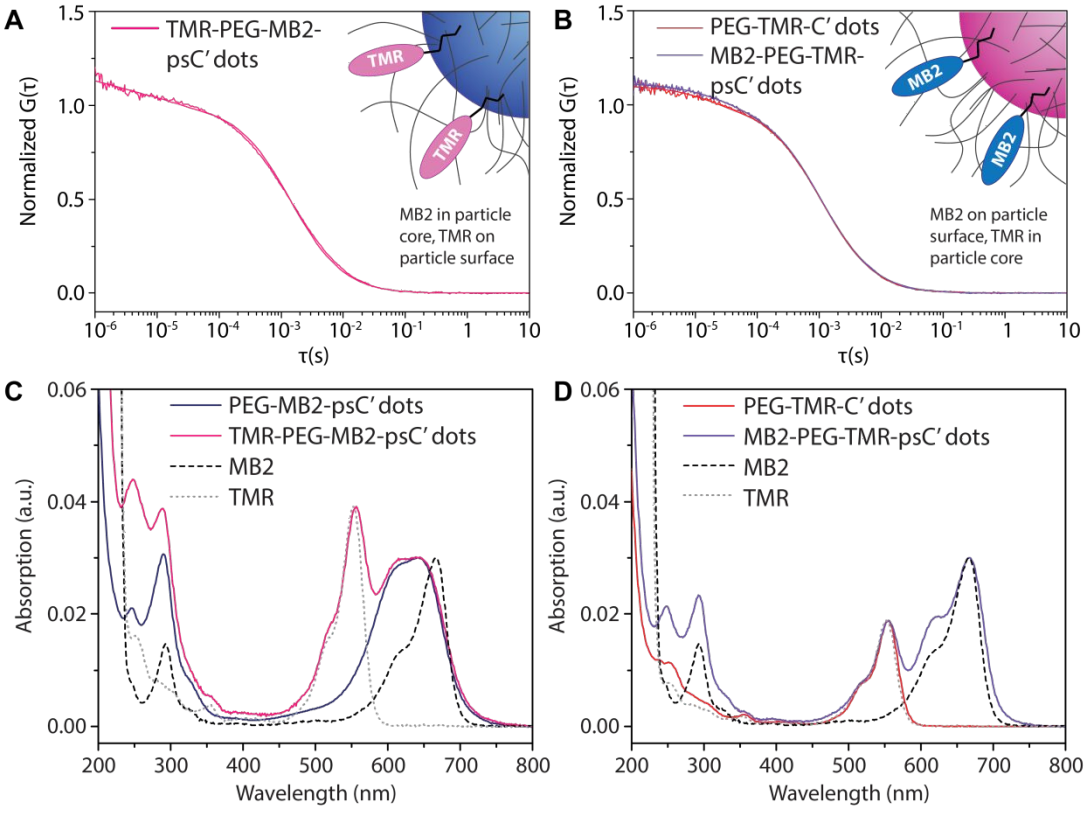

Figure 2. (A) and (C) FCS autocorrelation curve of MB2-PEG-TMR-psC'dot (design 1) and absorption spectra before and after TMR surface functionalization as compared to free TMR dye and MB2 photosensitizer. (B) and (D) FCS autocorrelation curves of PEG-TMR-C' dots and TMR-PEG-MB2-psC' dots (design 2) and absorption spectra before and after MB2 surface functionalization as compared to free TMR dye and MB2 photosensitizer.

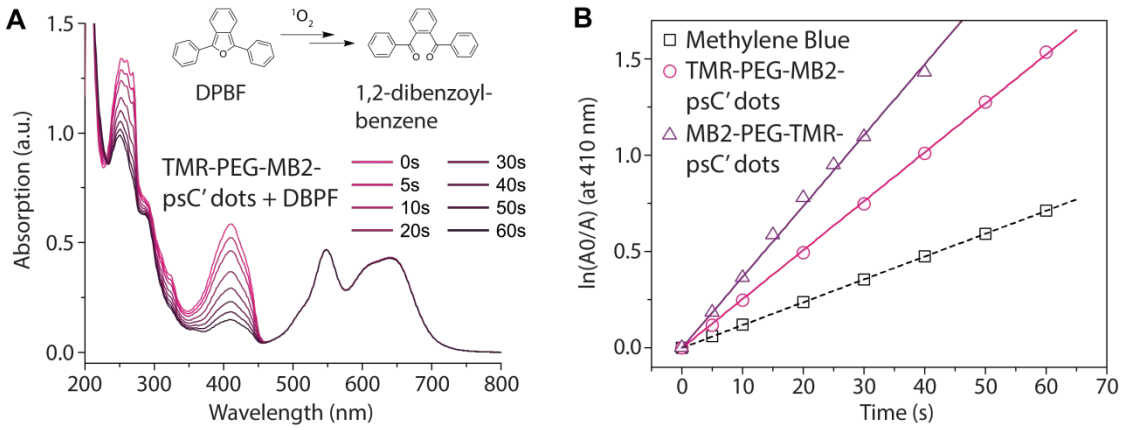

Figure 3. (A) Schematic representation of a photosensitizing measurement using 1,3-diphenylisobenzofuran (DPBF) as a singlet oxygen, $^1O_2$, sensor. Absorption of a solution containing TMR-PEG-MB2-psC' dots and DPBF irradiated at 635 nm for 60 s in intervals of 5 and 10 s (see legend). (B) Comparative $^1O_2$ generation of methylene blue, TMR-PEG-MB2-psC' dots, and MB2-PEG-TMR-psC' dots.

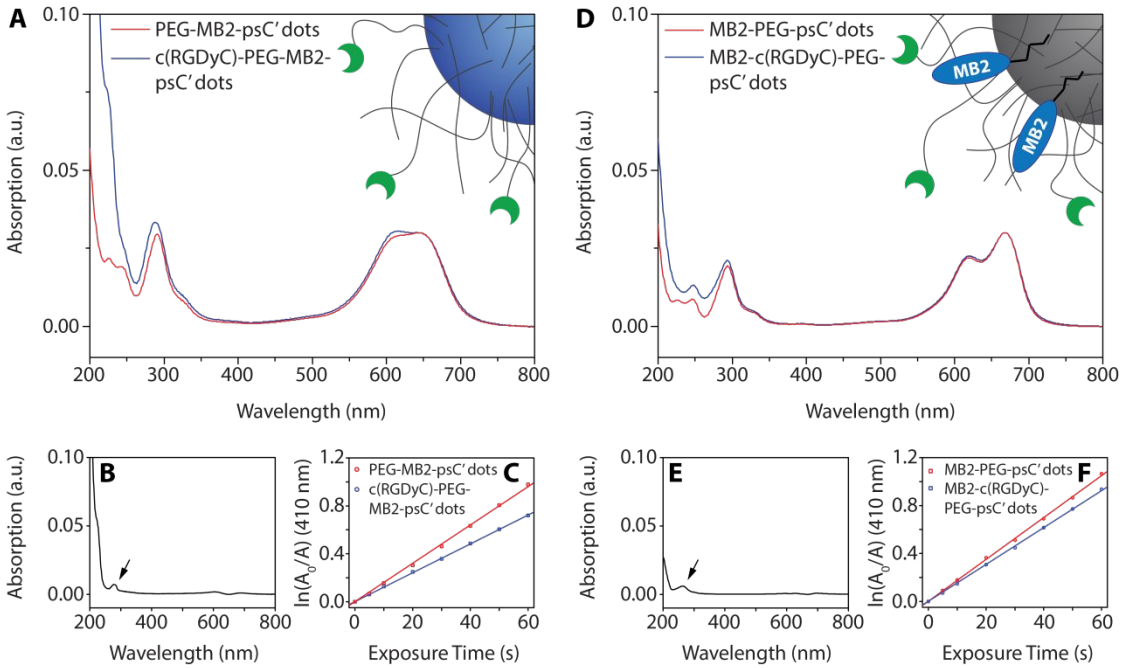

Figure 4. (A) Intensity matched absorption spectra of PEG-MB2-psC' dots and c(RGDyC)-PEG-MB2-psC' dots. (B) Difference spectrum of the two spectra in (A) revealing the absorption band of c(RGDyC). (C) Photosensitizing measurement of intensity matched PEG-MB2-psC' dots and c(RGDyC)-PEG-MB2-psC' dots. (D) Intensity matched absorption spectra of MB2-PEG-psC' dots and MB2-c(RGDyC)-PEG-PsC' dots. (E) Difference spectrum of the two spectra in (D) revealing the absorption band of c(RGDyC). (F) Photosensitizing measurement of intensity matched MB2-PEG-psC' dots and MB2-c(RGDyC)-PEG-psC' dots.

ASSOCIATED CONTENT

Supporting Information

Absorption spectra of MB and MB2, chemical structures of (cRGDyC)-PEG(12)-silane and MPTMS, comparative fluorescence emission spectra of free dye, C' dots and psC' dots, GPC elugrams before and after surface functionalization of psC' dots, TEM images of psC' dots, photobleaching experiments of MB2 and psC' dots.

AUTHOR INFORMATION

ORCID

Ferdinand F. E. Kohle: 0000-0002-7351-5940
Songying Li: 0000-0002-7977-9293
Melik Z. Turker: 0000-0001-7801-4275
Ulrich B. Wiesner: 0000-0001-6934-3755

Author Contributions

// F.F.E.K. and S.L. contributed equally to this paper.

Notes

The authors declare the following competing financial interest: F.F.E.K. and U.B.W. have filed for a patent based on these findings. Other authors declare no competing interests.

ACKNOWLEDGEMENTS

This work was funded by the National Institutes of Health (NIH) under Award

No. U54CA199081. It made use of the Cornell Center for Materials Research (CCMR) shared facilities which are supported through the NSF MRSEC program (DMR-1719875) at Cornell. The authors gratefully acknowledge L. Estroff (Cornell University) for helpful discussions.

REFERENCES

(1) Felsher, D. W. Cancer Revoked: Oncogenes as Therapeutic Targets. *Nat. Rev. Cancer* **2003**, *3* (5), 375–379. DOI: 10.1038/nrc1070

(2) Ochsner, M. Photophysical and Photobiological Processes in the Photodynamic Therapy of Tumours. *J. Photochem. Photobiol. B Biol.* **1997**, *39* (1), 1–18. DOI: 10.1016/s1011-1344(96)07428-3

(3) DeRosa, M. C.; Crutchley, R. J. Photosensitized Singlet Oxygen and Its Applications. *Coord. Chem. Rev.* **2002**, *233–234*, 351–371. DOI: 10.1016/S0010-8545(02)00034-6

(4) Agostinis, P.; Berg, K.; Cengel, K. A.; Foster, T. H.; Girotti, A. W.; Gollnick, S. O.; Hahn, S. M.; Hamblin, M. R.; Juzeniene, A.; Kessel, D.; Korbelik, M.; Moan, J.; Mroz, P.; Nowis, D.; Piette, J.; Wilson, B. C. Golab, J. Photodynamic Therapy of Cancer : An Update. *Am. Cancer Soc.* **2011**, *61* (4), 250–281. DOI: 10.3322/caac.20114

(5) Ormond, A. B.; Freeman, H. S. Dye Sensitizers for Photodynamic Therapy. *Materials* **2013**, *6* (3), 817–840. DOI: 10.3390/ma6030817

(6) Mehraban, N.; Freeman, H. S. Developments in PDT Sensitizers for Increased Selectivity and Singlet Oxygen Production. *Materials* **2015**, *8* (7), 4421-4456. DOI: 10.3390/ma8074421

(7) Singh, R.; Lillard, J. W. Nanoparticle-Based Targeted Drug Delivery. *Exp. Mol. Pathol.* **2009**, *86* (3), 215–223. DOI: 10.1016/j.yexmp.2008.12.004

(8) Peer, D.; Karp, J. M.; Hong, S.; Farokhzad, O. C.; Margalit, R.; Langer, R. Nanocarriers as an Emerging Platform for Cancer Therapy. *Nat. Nanotechnol.* **2007**, *2*, 751-760. DOI: 10.1038/nnano.2007.387

(9) Hartshorn, C. M.; Bradbury, M. S.; Lanza, G. M.; Nel, A. E.; Rao, J.; Wang, A. Z.; Wiesner, U. B.; Yang, L.; Grodzinski, P. Nanotechnology Strategies To Advance Outcomes in Clinical Cancer Care. *ACS Nano* **2018**, *12* (1), 24–43. DOI: 10.1021/acsnano.7b05108

(10) Bobo, D.; Robinson, K. J.; Islam, J.; Thurecht, K. J.; Corrie, S. R. Nanoparticle-Based Medicines: A Review of FDA-Approved Materials and Clinical Trials to Date. *Pharm. Res.* **2016**, *33* (10), 2373–2387. DOI: 10.1007/s11095-016-1958-5

(11) Lismont, M.; Dreesen, L.; Wuttke, S. Metal-Organic Framework Nanoparticles in Photodynamic Therapy: Current Status and Perspectives. *Adv. Funct. Mater.* **2017**, *27* (14), 1–16. DOI: 10.1002/adfm.201606314

(12) Chen, F.; Ma, K.; Zhang, L.; Madajewski, B.; Zanzonico, P.; Sequeira, S.; Gonen, M.; Wiesner, U.; Bradbury, M. S. Target-or-Clear Zirconium-89 Labeled Silica Nanoparticles for Enhanced Cancer-Directed Uptake in Melanoma: A Comparison of Radiolabeling Strategies. *Chem. Mater.* **2017**, *29* (19), 8269–8281. DOI: 10.1021/acs.chemmater.7b02567

(13) Choi, S. H.; Liu, W.; Misra, P.; Tanaka, E.; Zimmer, J. P.; Itty Ipe, B.; Bawendi, M. G.; Frangioni, J. V. Renal Clearance of Quantum Dots. *Nat. Biotechnol.* **2007**, *25* (10), 1165–1170. DOI: 10.1038/nbt1340

(14) Zhong, H.; Chan, G.; Hu, Y.; Hu, H.; Ouyang, D. A Comprehensive Map of FDA-Approved Pharmaceutical Products. *Pharmaceutics*. **2018**, *10* (4), 263. DOI: 10.3390/pharmaceutics10040263

(15) D'Mello, S. R.; Cruz, C. N.; Chen, M.-L.; Kapoor, M.; Lee, S. L.; Tyner, K. M. The Evolving Landscape of Drug Products Containing Nanomaterials in the United States. *Nat. Nanotechnol.* **2017**, *12*, 523-529. DOI: 10.1038/nnano.2017.67

(16) Herz, E.; Ow, H.; Bonner, D.; Burns, A.; Wiesner, U. Dye Structure–Optical Property Correlations in near-Infrared Fluorescent Core-Shell Silica Nanoparticles. *J. Mater. Chem.* **2009**, *19* (35), 6341–6347. DOI: 10.1039/B902286D

(17) Herz, E.; Burns, A.; Bonner, D.; Wiesner, U. Large Stokes-Shift Fluorescent Silica Nanoparticles with Enhanced Emission Over Free Dye for Single Excitation Multiplexing. *Macromol. Rapid Commun.* **2009**, *30* (22), 1907–1910. DOI: 10.1002/marc.200900389

(18) Ma, K.; Mendoza, C.; Hanson, M.; Werner-Zwanziger, U.; Zwanziger, J.;

Wiesner, U. Control of Ultrasmall Sub-10 nm Ligand-Functionalized Fluorescent Core-Shell Silica Nanoparticle Growth in Water. *Chem. Mater.* **2015**, *27* (11), 4119–4133. DOI: 10.1021/acs.chemmater.5b01222

(19) Burns, A. a; Vider, J.; Ow, H.; Herz, E.; Penate-medina, O.; Baumgart, M.; Larson, S. M.; Wiesner, U.; Bradbury, M. Fluorescent Silica Nanoparticles with Efficient Urinary Excretion for Nanomedicine. *Nano Lett.* **2009**, *9* (1), 442–448. DOI: 10.1021/nl803405h

(20) Phillips, E.; Penate-Medina, O.; Zanzonico, P. B.; Carvajal, R. D.; Mohan, P.; Ye, Y.; Humm, J.; Gönen, M.; Kalaigian, H.; Schöder, H.; Strauss, H.W.; Larson, S. M.; Wiesner, U.; Bradbury, M. S. Clinical Translation of an Ultrasmall Inorganic Optical-PET Imaging Nanoparticle Probe. *Sci. Transl. Med.* **2014**, *6* (260), 260ra149. DOI: 10.1126/scitranslmed.3009524

(21) Ma, K.; Werner-Zwanziger, U.; Zwanziger, J.; Wiesner, U. Controlling Growth of Ultrasmall Sub-10 nm Fluorescent Mesoporous Silica Nanoparticles. *Chem. Mater.* **2013**, *25* (5), 677–691. DOI: 10.1021/cm303242h

(22) Ma, K.; Gong, Y.; Aubert, T.; Turker, M. Z.; Kao, T.; Doerschuk, P. C.; Wiesner, U. Self-Assembly of Highly Symmetrical, Ultrasmall Inorganic Cages Directed by Surfactant Micelles. *Nature* **2018**, *558* (7711), 577–580. DOI: 10.1038/s41586-018-0221-0

(23) Ma, K.; Spoth, K. A.; Cong, Y.; Zhang, D.; Aubert, T.; Turker, M. Z.; Kourkoutis, L. F.; Mendes, E.; Wiesner, U. Early Formation Pathways of Surfactant Micelle Directed Ultrasmall Silica Ring and Cage Structures. *J. Am. Chem. Soc.* **2018**, *140* (50), 17343–17348. DOI: 10.1021/jacs.8b08802

(24) Ma, K.; Wiesner, U. Modular and Orthogonal Post-PEGylation Surface Modifications by Insertion Enabling Penta-Functional Ultrasmall Organic-Silica Hybrid Nanoparticles. *Chem. Mater.* **2017**, *29* (16), 6840–6855. DOI: 10.1021/acs.chemmater.7b02009

(25) Chen, F.; Ma, K.; Madajewski, B.; Zhuang, L.; Zhang, L.; Rickert, K.; Marelli, M.; Yoo, B.; Turker, M. Z.; Overholtzer, M.; Quinn, T. P.; Gonen, M.; Zanzonico, P.; Tuesca, A.; Bowen, M. A.; Norton, L.; Subramony, J. A. Wiesner, U.; Bradbury, M. S. Ultrasmall Targeted Nanoparticles with Engineered Antibody Fragments for Imaging Detection of HER2-Overexpressing Breast Cancer. *Nat. Commun.* **2018**, *9* (1), 4141. DOI: 10.1038/s41467-018-06271-5

(26) Farrell, A. T. NDA 204630, Center for Drug Evaluation and Research, Beltsville, **2016**.

(27) Tardivo, J. P.; Giglio, A. Del; Santos De Oliveira, C.; Santesso Gabrielli, D.; Couto Junqueira, H.; Tada, D. B.; Severino, D.; De Fátima Turchiello, R.; Baptista Phd, M. S. Methylene Blue in Photodynamic Therapy: From Basic Mechanisms to Clinical Applications. *Photodiagnosis Photodyn. Ther.* **2005**, *2* (3), 175–191. DOI: 10.1016/S1572-1000(05)00097-9

(28) ATTO-TEC Product Information: ATTO MB2, https://www.atto-tec.com/fileadmin/user_upload/Katalog_Flyer_Support/ATTO_MB2.pdf, (8/24/2019).

(29) Lucky, S. S.; Soo, K. C.; Zhang, Y. Nanoparticles in Photodynamic Therapy. *Chem. Rev.* **2015**, *115* (4), 1990–2042. DOI: 10.1021/cr5004198

(30) Tang, W.; Xu, H.; Kopelman, R.; A. Philbert, M. Photodynamic Characterization and In Vitro Application of Methylene Blue-Containing Nanoparticle Platforms. *Photochem. Photobiol.* **2005**, *81* (2), 242–249. DOI: DOI: 10.1562/2004-05-24-RA-176.1

(31) Qin, M.; Hah, H. J.; Kim, G.; Nie, G.; Lee, Y.-E. K.; Kopelman, R. Methylene Blue Covalently Loaded Polyacrylamide Nanoparticles for Enhanced Tumor-Targeted Photodynamic Therapy. *Photochem. Photobiol. Sci.* **2011**, *10* (5), 832–841. DOI: 10.1039/c1pp05022b

(32) Kohle, F. F. E.; Hinckley, J. A.; Li, S.; Dhawan, N.; Katt, W. P.; Erstling, J. A.; Werner-Zwanziger, U.; Zwanziger, J.; Cerione, R. A.; Wiesner, U. B. Amorphous Quantum Nanomaterials. *Adv. Mater.* **2019**, *31* (5), 1806993. DOI: 10.1002/adma.201806993

(33) Benezra, M.; Penate-Medina, O.; Zanzonico, P. B.; Schaer, D.; Ow, H.; Burns, A.; DeStanchina, E.; Longo, V.; Herz, E.; Iyer, S.; Wolchok, J.; Larson, S. M.; Wiesner, U.; Bradbury, M. S. Multimodal Silica Nanoparticles Are Effective Cancer-Targeted Probes in a Model of Human Melanoma. *J. Clin. Invest.* **2011**, *121* (7), 2768–2780. DOI: 10.1172/JCI45600

(34) Chen, F.; Ma, K.; Benezra, M.; Zhang, L.; Cheal, S. M.; Phillips, E.; Yoo, B.; Pauliah, M.; Overholtzer, M.; Zanzonico, P.; Sequeira, S.; Gonen, M.; Quinn, T.; Wiesner, U.; Bradbury, M. S. Cancer-Targeting Ultrasmall Silica Nanoparticles for Clinical Translation: Physicochemical Structure and Biological Property Correlations. *Chem. Mater.* **2017**, *29* (20), 8766–8779. DOI: 10.1021/acs.chemmater.7b03033

(35) Ma, K.; Zhang, D.; Cong, Y.; Wiesner, U. Elucidating the Mechanism of Silica Nanoparticle PEGylation Processes Using Fluorescence Correlation Spectroscopies. *Chem. Mater.* **2016**, *28* (5), 1537–1545. DOI: 10.1021/acs.chemmater.6b00030

(36) Larson, D. R.; Ow, H.; Vishwasrao, H. D.; Heikal, A. A.; Wiesner, U.; Webb, W. W. Silica Nanoparticle Architecture Determines Radiative Properties of Encapsulated Fluorophores. *Chem. Mater.* **2008**, *20* (8), 2677–2684. DOI: 10.1021/cm7026866

(37) Kohle, F. F. E.; Hinckley, J. A.; Wiesner, U. B. Dye Encapsulation in Fluorescent Core–Shell Silica Nanoparticles as Probed by Fluorescence Correlation Spectroscopy. *J. Phys. Chem. C* **2019**, *123* (15), 9813–9823. DOI: 10.1021/acs.jpcc.9b00297

(38) Redmond, R. W.; Gamlin, J. N. A Compilation of Singlet Oxygen Yields from Biologically Relevant Molecules. *Photochem. Photobiol.* **1999**, *70* (4), 391–475.

(39) Yogi, C.; Kojima, K.; Wada, N.; Tokumoto, H.; Takai, T.; Mizoguchi, T.; Tamiaki, H. Photocatalytic Degradation of Methylene Blue by TiO2film and Au Particles-TiO2composite Film. *Thin Solid Films* **2008**, *516* (17), 5881–5884. DOI: 10.1016/j.tsf.2007.10.050

(40) Marbán, G.; Vu, T. T.; Valdés-Solís, T. A Simple Visible Spectrum Deconvolution Technique to Prevent the Artefact Induced by the Hypsochromic Shift from Masking the Concentration of Methylene Blue in Photodegradation Experiments. *Appl. Catal. A Gen.* **2011**, *402* (1–2), 218–223. DOI: 10.1016/j.apcata.2011.06.009

(41) Patil, K.; Pawar, R.; Talap, P. Self-Aggregation of Methylene Blue in Aqueous Medium and Aqueous Solutions of Bu4NBr and Urea. *Phys. Chem. Chem. Phys.* **2000**, *2* (19), 4313–4317. DOI: 10.1039/B005370H

(42) Junqueira, H. C.; Severino, D.; Dias, L. G.; Gugliotti, M. S.; Baptista, M. S. Modulation of Methylene Blue Photochemical Properties Based on Adsorption at Aqueous Micelle Interfaces. *Phys. Chem. Chem. Phys.* **2002**, *4* (11), 2320–2328. DOI: 10.1039/B109753A

(43) Severino, D.; Junqueira, H. C.; Gugliotti, M.; Gabrielli, D. S.; Baptista, M. S. Influence of Negatively Charged Interfaces on the Ground and Excited State Properties of Methylene Blue. *Photochem. Photobiol.* **2003**, *77* (5), 459–468. DOI: 10.1562/0031-8655(2003)077<0459:ioncio>2.0.co;2

(44) Carloni, P.; Damiani, E.; Greci, L.; Stipa, P.; Tanfani, F.; Tartaglini, E.; Wozniak, M. On the Use of 1,3-Diphenylisobenzofuran (DPBF). Reactions with Carbon and Oxygen Centered Radicals in Model and Natural Systems. *Res. Chem. Intermed.* **1993**, *19* (5), 395–405. DOI: 10.1163/156856793X

(45) Nuñez, S. C.; Yoshimura, T. M.; Ribeiro, M. S.; Junqueira, H. C.; Maciel, C.; Coutinho-Neto, M. D.; Baptista, M. S. Urea Enhances the Photodynamic Efficiency of Methylene Blue. *J. Photochem. Photobiol. B Biol.* **2015**, *150*, 31–37. DOI: 10.1016/j.jphotobiol.2015.03.018

(46) Ow, H.; Larson, D. R.; Srivastava, M.; Baird, B. A.; Webb, W. W.; Wiesnert, U. Bright and Stable Core-Shell Fluorescent Silica Nanoparticles. *Nano Lett.* **2005**, *5* (1), 113–117. DOI: 10.1021/nl0482478

(47) Mundra, V.; Li, W.; Mahato, R. I. Nanoparticle-Mediated Drug Delivery for Treating Melanoma. *Nanomedicine* **2015**, *10* (16), 2613–2633. DOI: 10.2217/nnm.15.111

(48) Kang, W.; Svirskis, D.; Sarojini, V.; McGregor, A. L.; Bevitt, J.; Wu, Z. Cyclic-RGDyC Functionalized Liposomes for Dual-Targeting of Tumor Vasculature and Cancer Cells in Glioblastoma: An in Vitro Boron Neutron Capture Therapy Study. *Oncotarget* **2017**, *8* (22), 36614–36627. DOI: 10.18632/oncotarget.16625

TABLE OF CONTENTS GRAPHIC

For Table of Contents Use Only.

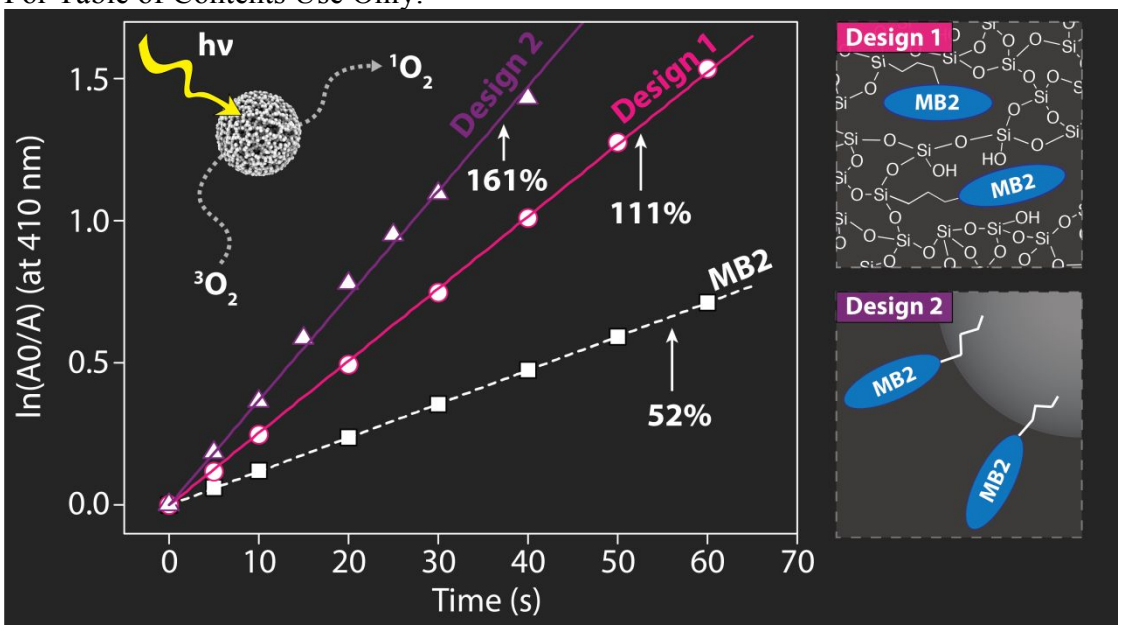

Title: Ultrasmall PEGylated and Targeted Core-Shell Silica Nanoparticles Carrying Methylene Blue Photosensitizer

Authors: Ferdinand F. E. Kohle, Songying Li, Melik Z. Turker, and Ulrich B. Wiesner